

L.W. LU\* W.G. QIN\*

**CHARACTERIZATIONS AND EVALUATIONS ON THE BONDING QUALITY OF MOLYBDENUM DISILICIDES****CHARAKTERYSTYKA I OCENA JAKOŚCI POŁĄCZEŃ WYTWORZONYCH PRZEZ MoSi<sub>2</sub>**

In this study, we proposed a new method using the spark plasma sintering technique to bond ceramics to alloys. MoSi<sub>2</sub> and 316L stainless steel were chosen as sample materials and can be welded well with graded interlayers. We found that dense uniformed bondings were achieved because of the comparable coefficient of thermal expansion of the interlayers. Furthermore, such a compatibility between the graded interlayers prevented MoSi<sub>2</sub> with low toughness from the occurrence of microcracks resulted from the residual stresses formed during cooling of the bondings.

*Keywords:* MoSi<sub>2</sub>; 316L Stainless steel; Bonding; Sintering

W pracy zaproponowano nową metodę łączenia ceramiki i stopów metodą spiekania iskrowo plazmowego SPS (spark plasma sintering). MoSi<sub>2</sub> i stal nierdzewna 316L zostały wybrane jako przykładowe materiały i mogą być łączone poprzez gradientowe warstwy pośrednie. Okazało się, że zwarte, jednorodne połączenia zostały uzyskane dzięki porównywalnemu współczynnikowi rozszerzalności cieplnej warstw pośrednich. Ponadto, tego rodzaju zgodność pomiędzy warstwami pośrednimi zapobiegła wystąpieniu mikropęknięć w MoSi<sub>2</sub>, który jest materiałem o niskiej twardości, będących wynikiem naprężeń powstałych podczas chłodzenia połączeń.

**1. Introduction**

Ceramics such as molybdenum disilicides (MoSi<sub>2</sub>) are very promising for structural applications at high temperatures because of their high melting point (T<sub>m</sub>=2030°), moderate density, excellent oxidation resistance, good electrical conductivity and stability in a variety of corrosive environments [1-2]. There are several potential applications that have been identified for MoSi<sub>2</sub> in the aerospace, automotive, energy sources and so on [3-4].

In order for MoSi<sub>2</sub> to be used in various industries, it is necessary to bond it to other materials, such as ferrous and non-ferrous alloys, since such ceramics are generally brittle. However, direct welding of MoSi<sub>2</sub> to most metals and alloys is not possible owing to differences in CTE and the necessity for high bonding temperatures, which can lead to joint failure upon cooling because of large residual stresses. To solve this issue, efforts have been made to employ various welding/bonding techniques. For example, Conzone et al. [5] first used active brazing techniques to obtain the tense uniformed

joints of MoSi<sub>2</sub> to 316L; however, the Cu/Si phase produced at the MoSi<sub>2</sub>/Nb interface limits the use temperature of MoSi<sub>2</sub>/316L joints because it has a relatively low melting temperature (852°) and the successful use of this joint at temperatures approaching 852° could only be achieved in a non-oxidizing environment.

The spark plasma sintering (SPS) technique is a simple and promising method for materials processing. It is considerably practical and may be applicable in various industries to reduce the thermal stresses of joints if suitable technological parameters are adopted. Especially, to better exert the advantage of this technique, it is simple and convenient to design various graded material interlayers in order to improve the compatibility of different materials and to reduce the thermal stresses of each layer. It is worth noting that efforts have been made to apply the SPS technique to bonding different materials since the last decade. For example, Fan et al. [6] bonded Mo to CoSb<sub>3</sub> using SPS by inserting a Ti interlayer, whereas Liu et al. [7] bonded dissimilar nanocrystalline materials by a reactive synthesis. In the above studies, generally, the joint with excellent properties was achieved at mod-

\* DEPARTMENT OF BIOLOGICAL AND CHEMICAL ENGINEERING, HUNAN MECHANICAL & ELECTRICAL POLYTECHNIC, CHANGSHA 410151, P. R. CHINA

erate temperatures. However, the residual thermal stress induced during cooling, a decisive factor in the bonding strength in the graded interlayer, can always occur and is hardly effectively and accurately measured by X-RAY and other conventional methods [8-11].

In this work, we developed a new approach of SPS by the use of 9 graded interlayers to bond  $\text{MoSi}_2$  to 316L stainless steel. The joint with excellent properties was achieved at moderate temperatures.

## 2. Experimental procedure

99.0%  $\text{MoSi}_2$  ( $<10\mu\text{m}$ ), 99.9%  $\text{ZrO}_2$  (40nm), and 98.0% 316L stainless steel ( $165\mu\text{m}$ ) powders were purchased from the local commercial company. Table 1 gives the chemical compositions of 316L powders. According to the design of 9 interlayers (Fig. 1), the volume fraction of  $\text{MoSi}_2$  / 316L graded interlayers was obtained, as shown in Table 2. Powders of each layer were mixed in agate ball grinding cans in a planetary ball miller (QM-SB type) for 4h. The resulting powder mixtures were then cold pressed layer by layer in a graphite die ( $\phi 20\text{mm} \times 55\text{ mm}$ ). Perfect chemical bonding can be achieved when a sintering process is completed in the die. The entire powder assembly was sintered in a SPS furnace, as shown in Fig. 2. Figure 3 illustrates variations in temperature with time during a sintering process.

TABLE 1

Chemical compositions of 316L stainless steel (Wt%)

| C            | Si          | Mn          | P            | S            | Ni    | Cr   | Mo   |
|--------------|-------------|-------------|--------------|--------------|-------|------|------|
| $\leq 0.030$ | $\leq 1.00$ | $\leq 2.00$ | $\leq 0.035$ | $\leq 0.030$ | 10.35 | 17.4 | 2.89 |

TABLE 2

Volume fraction of  $\text{MoSi}_2$  / 316L graded interlayers

| Layer | 316L stainless steel powder | $\text{MoSi}_2$ powder |
|-------|-----------------------------|------------------------|
| A     | 90.10                       | 9.90                   |
| B     | 76.15                       | 23.85                  |
| C     | 64.11                       | 35.89                  |
| D     | 53.03                       | 46.97                  |
| E     | 42.57                       | 57.43                  |
| F     | 32.56                       | 67.44                  |
| G     | 22.92                       | 77.08                  |
| H     | 13.57                       | 86.43                  |
| I     | 4.47                        | 95.53                  |

The specimens after sintering process were characterized using a conventional optical microscope. For microstructural observations, joints were cut off along the cross-section, and then the specimens were first polished using 320# sand paper (SiC, particle size:  $40\mu\text{m}$ ) and then using  $0.05\mu\text{m}$  colloidal silica to get a mirror-finish surface. The polished surfaces were etched with  $\text{FeCl}_3+\text{HCl}$ , HF and  $\text{HNO}_3$  solutions for 5s, respectively, in order to remove the contaminated layer caused by polishing. All the specimens were finally cleaned using an ultrasonic cleaner with reagent grade acetone (for 10min) and reagent alcohol (for 5min), and then dried in an inert container.

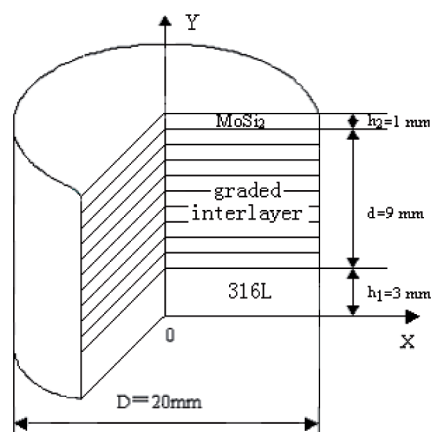


Fig. 1. Distribution and dimension of different gradient interlayers

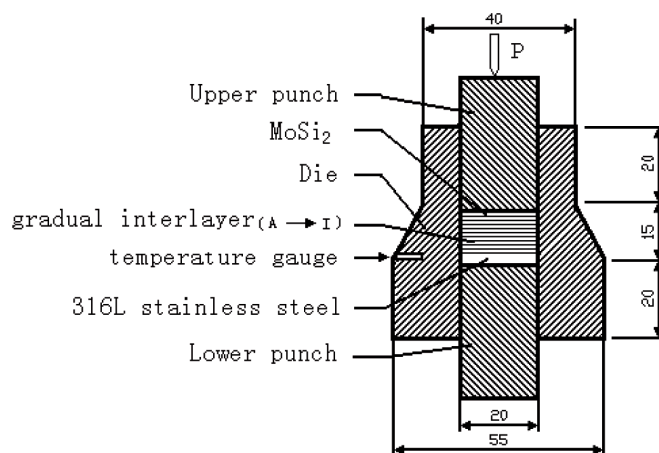


Fig. 2. Schematic illustration of the sintering processing of the graded interlayers

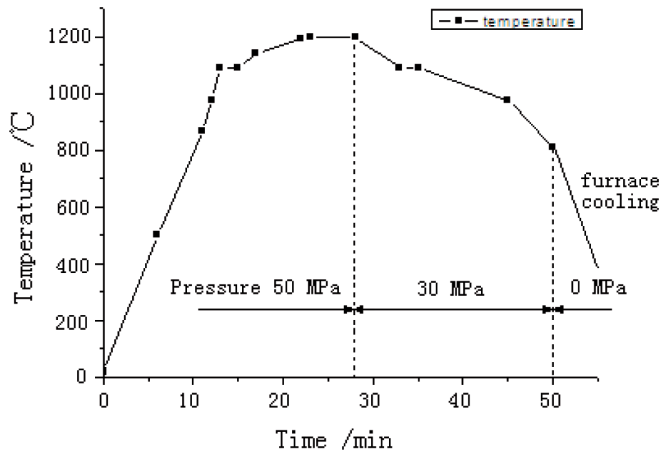


Fig. 3. Variations in temperature with time during a sintering process

### 3. Results and discussion

#### 3.1. Microstructural observations

The metallurgical morphology of a joint produced using nine MoSi<sub>2</sub>/316L graded interlayers is shown

in Fig. 4. As shown, the microstructure of the joint is arranged at 316L/A/B/.../I/ 10% ZrO<sub>2</sub>-MoSi<sub>2</sub> from left to right, and the interfaces between layers are not clear marked, indicating that the composition of layers is changed slowly and the interfaces are bonding well. It is also seen that the graded interlayer produced a joint without microcracks or porosities. It was demonstrated previously [9] that in general, the occurrence of microcracks in joints was a result of large stresses developing due to the CTE mismatching between the materials being bonded. However, in the present study, CTE would be expected to be changed slowly because of gradient compositions within layer by layer. Accordingly, residual stress produced by cooling would be expected to be reduced largely. On the other hand, plastic deformation within the interlayers of a joint is one mechanism that can partially relieve these stresses, according to finite element analysis and experimental findings previously [1, 2], when residual stress is larger than the yield strength of materials, microcrack and failure in the joint would be produced through the low-toughness MoSi<sub>2</sub>.

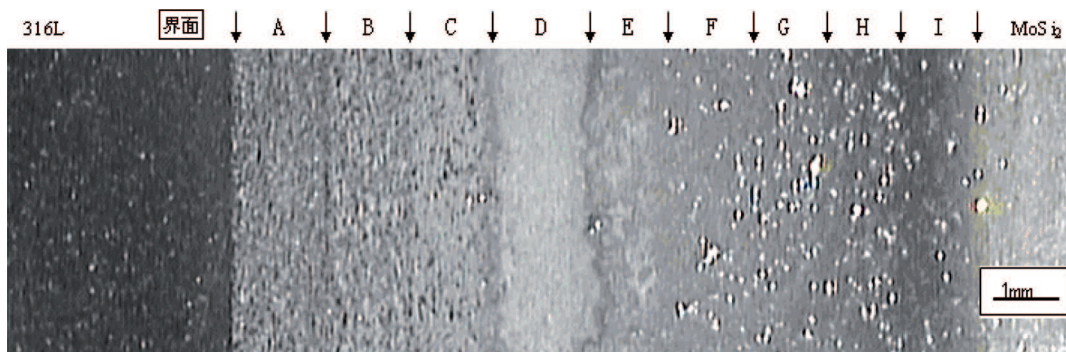
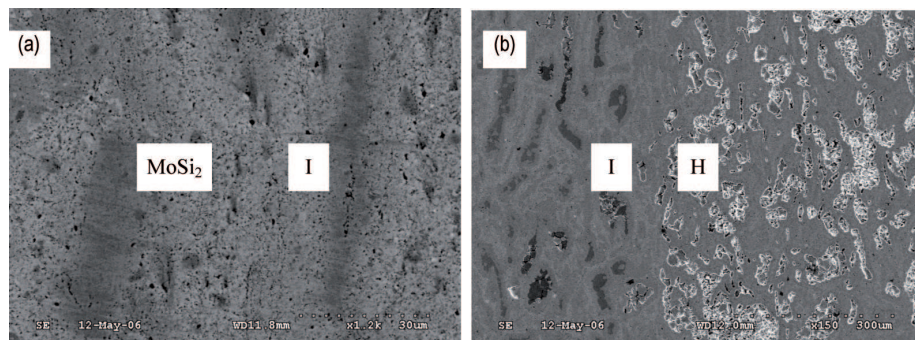


Fig. 4. A typical optical microstructural image of the MoSi<sub>2</sub>/316L bondings





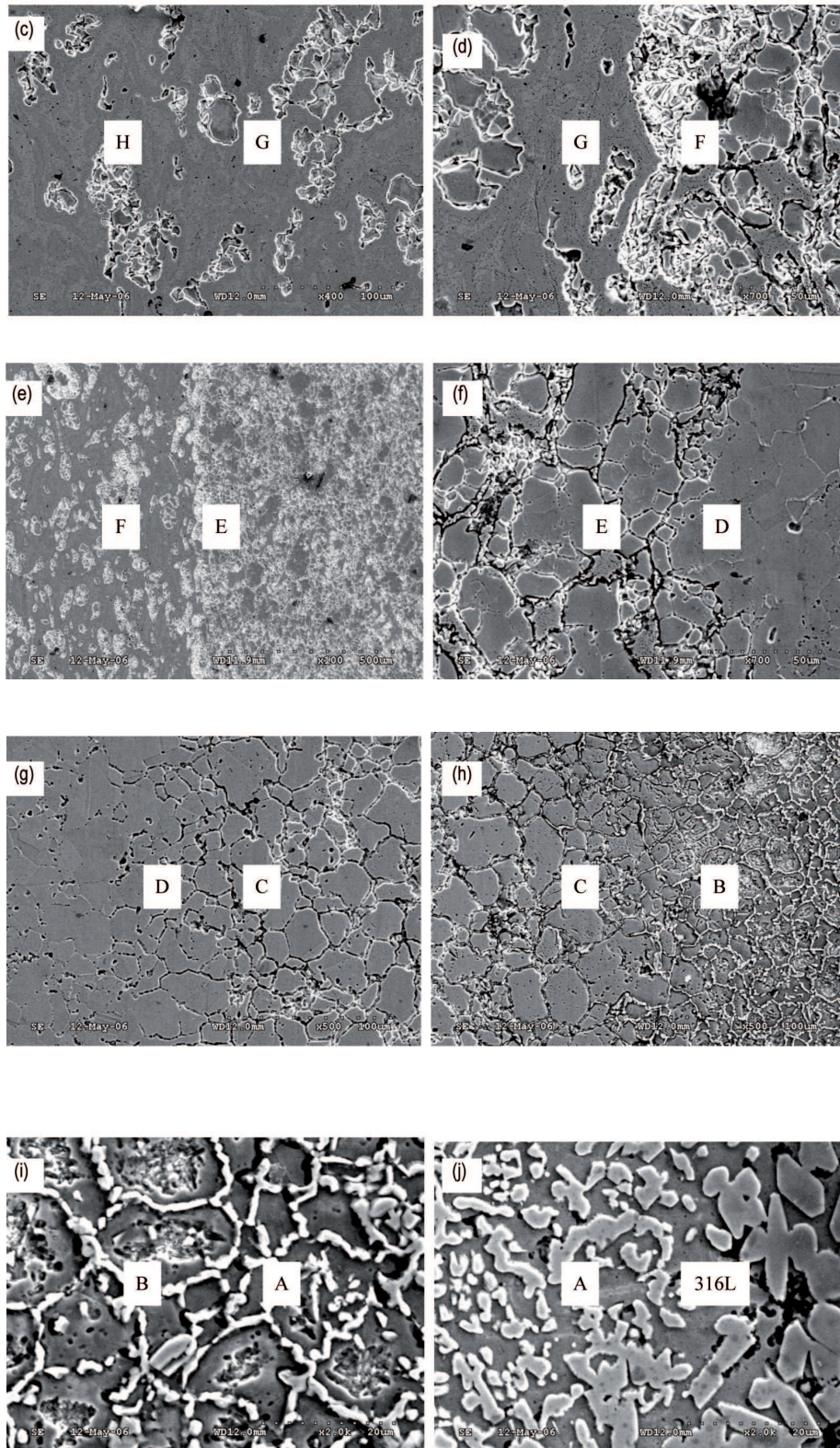


Fig. 5. SEM micrographs of the different interfaces (a-j) of graded interlayers within the joint

The SEM observations of the interfaces of graded interlayers within the joint are shown in Fig. 5. It is seen that no macroscopic defects in the interfaces of MoSi<sub>2</sub>-I,

I-H, H-G, F-E, C-B, B-A, and A-316L are found; instead, there exists only the continuous graded distribution of components with tightly bonded interfaces, yet the os-



tensible gap is found in the grain boundaries between the interfaces E-D and D-C, probably due to the granule dropping or the pulling out there. At the B-F layer, most of  $\text{MoSi}_2$  are distributed at the grain boundary in the form of network, only a few are dissolved into the stainless steel substrate, which is consistent with the result based on the spectrometric analysis, as illustrated in Fig. 6.

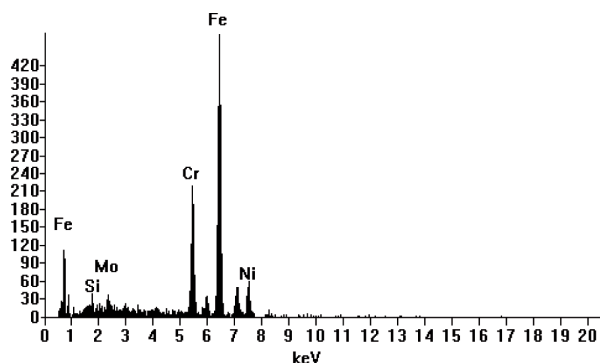


Fig. 6. Result for the spectrometric analysis of component

### 3.2. Discussion

Figure 7 shows a typical image for the occurrence of crack. As seen, the crack is pulled out around the free boundary near the interfaces between  $\text{MoSi}_2$  and the graded layers. As indicated in the earlier finite element analysis, this happens because the maximum axial tension stress can form at the boundary during cooling.

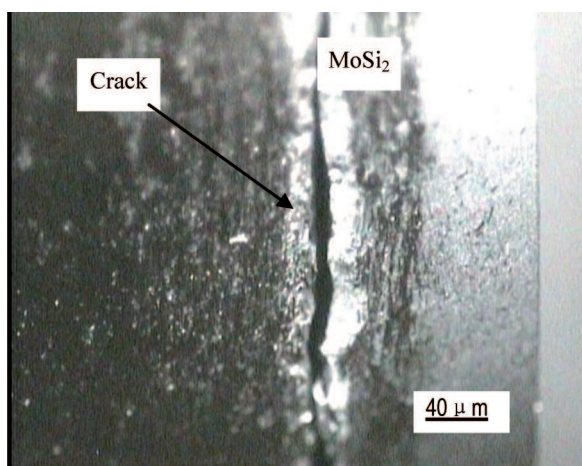


Fig. 7. A typical crack due to the axial stress

Correspondingly, it is experimentally found that most cracks initiate and grow on the  $\text{MoSi}_2$  surface and then extend gradually toward the substrate along a direction vertical to the boundary (Fig. 8). To avoid the occurrence of cracks and to design ideal or optimal interfacial or boundary microstructures, a comprehensive consideration of the number of layers, and the composition

and thickness of each layer is required. In particular, because the substrate (steel) has higher toughness and can resist the tension stress more effectively than  $\text{MoSi}_2$ , it is practical to employ both theoretical and experimental approaches to explore a suitable the compositional exponent in order to minimize the residual thermal tension stress. In addition, while optimizing the compositional exponent of graded layers, it is also need to further simplify the technology to reduce the cost of various raw materials.

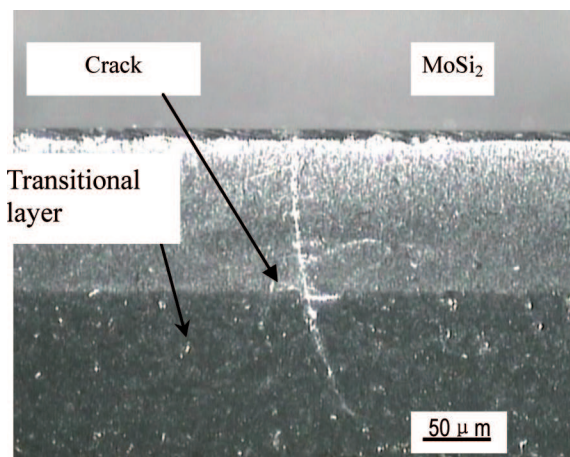


Fig. 8. A typical crack due to the radial stress

### 4. Conclusion

A new approach has been proposed to bond  $\text{MoSi}_2$  to 316L stainless steel using the spark plasma sintering (SPS) technique. Furthermore, a  $\text{MoSi}_2$ /316L gradient material has been designed and the resultant compact uniformed joint with few cracks has been achieved because of the matching of thermal expansion coefficient between  $\text{MoSi}_2$  and the graded interlayers.

### REFERENCES

- [1] J. Kuchino, K. Kurokawa, T. Shibayama, et al. *Vacuum* **73**, 623-628 (2004).
- [2] H. Zhang, C. Long, P. Chen, et al. *Inter. J. Refractory Met. Hard Mater.* **21**, 75-79 (2003).
- [3] R.G. Castro, et al. *Mater. Sci. Eng.* **A185**, 65-70 (1994).
- [4] J. Jetrovic, *Mater. Sci. Eng.* **A192/A193**, 31-37 (1995).
- [5] S.D. Conzone, D.P. Butt, A.H. Bartlett, *J. Mater. Sci.* **32**, 3369-3374 (1997).
- [6] J.F. Fan, L.D. Chen, S.Q. Bai, X. Shi, *Mater. Lett.* **58**, 3876-3878 (2004).
- [7] W.P. Liu, M. Naka, *Scr. Mater.* **48**, 1225-1230 (2003).

- [8] M.H. Yu, D.B. Bi, B. Zhou, *Mech. Mater.* **12**, 65-69 (2005). (in Chinese).
- [9] R.U. Vaidya, et al. *Acta mater.* **46**, 6, 2047-2061 (1998).
- [10] Y. Xu, D. Tu, X. Li, *Mater. Mech. Eng.* **28**, 7, 15-17 (2004).
- [11] Y. Li, Y. Wang, *Mater. Mech. Eng.* **27**, 2, 14-16 (2003).

*Received: 20 March 2011.*